Hydrodynamic behavior of the pseudopotential lattice Boltzmann method for interfacial flows

Hydrodynamic behavior of the pseudopotential lattice Boltzmann method for interfacial flows

Daniele Chiappini*
Department of Industrial Engineering, University of Rome "Niccolò Cusano," Via don Carlo Gnocchi 3, 00166 Rome, Italy

Mauro Sbragaglia
Department of Physics, INFN, University of Rome "Tor Vergata," Via della Ricerca Scientifica 1, 00133 Rome, Italy

Xiao Xue
Department of Physics, INFN, University of Rome "Tor Vergata," Via della Ricerca Scientifica 1, 00133 Rome, Italy and Department of Physics, Eindhoven University of Technology, 5600 MB Eindhoven, The Netherlands

Giacomo Falcucci
Department of Enterprise Engineering "Mario Lucertini," University of Rome "Tor Vergata," Via del Politecnico 1, 00133 Rome, Italy and John A. Paulson School of Engineering and Applied Physics, Harvard University, 33 Oxford Street, 02138 Cambridge, Massachusetts, USA

(Received 10 December 2018; published 17 May 2019)

The lattice Boltzmann method (LBM) is routinely employed in the simulation of complex multiphase flows comprising bulk phases separated by nonideal interfaces. The LBM is intrinsically mesoscale with a hydrodynamic equivalence popularly set by the Chapman-Enskog analysis, requiring that fields slowly vary in space and time. The latter assumptions become questionable close to interfaces where the method is also known to be affected by spurious nonhydrodynamical contributions. This calls for quantitative hydrodynamical checks. In this paper, we analyze the hydrodynamic behavior of the LBM pseudopotential models for the problem of the breakup of a liquid ligament triggered by the Plateau-Rayleigh instability. Simulations are performed at fixed interface thickness, while increasing the ligament radius, i.e., in the "sharp interface" limit. The influence of different LBM collision operators is also assessed. We find that different distributions of spurious currents along the interface may change the outcome of the pseudopotential model simulations quite sensibly, which suggests that a proper fine-tuning of pseudopotential models in time-dependent problems is needed before the utilization in concrete applications. Taken all together, we argue that the results of the proposed paper provide a valuable insight for engineering pseudopotential model applications involving the hydrodynamics of liquid jets.

DOI: 10.1103/PhysRevE.99.053305

I. INTRODUCTION

The development of modern applications and innovative materials involving multiphase flows [1,2] naturally sets a compelling case for the development of suitably designed numerical methods to be used in synergy with experimental investigations [3] and analytical predictions [4]. The understanding of many of such problems is routinely rationalized via the help of a continuum hydrodynamics: In a nutshell, one can say that bulk phases coexist while being separated by thin interfaces, whose width represents the smallest scale of the continuum description. Such interfaces are characterized by a nonzero surface tension, i.e., the force per unit area that is the continuum manifestation of the anisotropy of atomistic forces close to the interface. Whereas for purely analytical calculations, the zero-width limit ("sharp interface" hydrodynamics) is most easily handable [5–7], for numerical simulations the situation is somehow more diversified [8–14]. In this landscape, increasing attention has been driven towards mesoscale simulations and, in particular, the lattice Boltzmann method (LBM) [15–20]. When solving the complex fluid dynamics of multiphase flows, the traditional advantages of the LBM (simplicity [21,22], easy handling of boundary conditions [23,24], and easy parallelization [25]) can be further enriched by a remarkable versatility in simulating nonideal equations of state (EoS) and complex interfaces [26,27]. More precisely, LBM reproduces "diffuse" interfaces, i.e., the bulk phases are separated by a region of finite thickness where the fluid properties (i.e., density, velocity, and pressure) change continuously. The hydrodynamical behavior of the LBM is traditionally assessed via the Chapman-Enskog analysis; however, from the theoretical point of view, the main assumptions of the Chapman-Enskog analysis of having fields slowly varying in space and time may well be violated due to the presence of the interfaces and/or singular events, such as breakups [28,29]. Practically, it is also found that LBM implementations are affected by spurious contributions at the interface [30,31]. We use the term spurious meaning that they are not predicted by hydrodynamics. These spurious currents are particularly relevant close to the interfaces [32]. Consequently, the actual recovery of the LBM-hydrodynamic

*daniele.chiappini@unicusano.it

"equivalence" could fail [15,33]. Natural questions then arise on the quantitative potentiality retained by diffuse interface LBM simulations of multiphase flows, especially in comparison to the analytical description of sharp interface hydrodynamics. In fact, although it is largely acknowledged in the literature [20,34–43] that the LBM is capable of reproducing static properties driven by surface tensions (i.e., Laplace pressures [44] and contact angles [45]), very rarely there have been quantitative characterizations on the recovery of time-dependent hydrodynamics with nonideal interfaces, especially in the presence of singular events. This paper aims to take a step forward in the latter direction. As a prototypical problem of a time-dependent multiphase flow with nonideal interfaces, we refer to the Plateau-Rayleigh instability [6,46–52] of a liquid ligament. The Plateau-Rayleigh instability—driven by the tendency of the interface to minimize the area at fixed available volume—causes the fragmentation of a liquid ligament into smaller droplets via breakup events. Numerical results on the breakup time show a neat asymptotic behavior when the interface width is much smaller than the ligament size. These asymptotic results are compared with the theoretical predictions of sharp interface hydrodynamics; moreover, our observations are also enriched with a side-by-side comparison of two different LBM collision operators, namely, the single relaxation time (SRT) with shifted equilibrium [30] and the multiple relaxation times (MRT) with Guo-like forcing [53]. Numerical simulations show that the distribution of velocity at the interface in the vicinity of the pinch-off region is different, causing different breakup processes. A very preliminary investigation on some of the results presented in this paper is also available in a recent conference proceedings [54].

The paper is organized as follows. In Sec. II, we recall the basic features of the numerical methodology used; in Sec. III, we report on the setup used for the numerical simulations; results will be presented in Sec. IV, and in Sec. V, conclusions will be drawn.

II. NUMERICAL MODELS

In this section, we briefly highlight the important features of the numerical methodology based on the LBM [15,19]. For extensive technical details, the interested reader is referred to the papers cited in the following. The LBM is a mesoscale numerical approach for the study of fluid dynamics, which has been successfully employed to dissect complex phenomena of scientific and technical interest in recent years [20,23,27,37,40,55,56].

The LBM is grounded on an optimized formulation of Boltzmann's kinetic equation in which particle distribution functions $f_\alpha(\mathbf{x},t)$ stream and collide on a lattice characterized by a finite set of velocities $\mathbf{c}_\alpha = 0,\ldots,18$ in our case, according to the following dynamics:

$$\begin{aligned}\Delta_\alpha f_\alpha(\mathbf{x},t) &= f_\alpha(\mathbf{x}+\mathbf{c}_\alpha\Delta t, t+\Delta t) - f_\alpha(\mathbf{x},t)\\ &= -\Omega_{\text{coll}}\left[f_\alpha(\mathbf{x},t) - f_\alpha^{\text{eq}}(\mathbf{x},t)\right]. \end{aligned} \tag{1}$$

In Eq. (1), Ω_{coll} represents the collision operator, which can be written as follows:

$$\begin{aligned}\Omega_{\text{coll}} &= \Delta t/\tau \quad \text{(SRT)},\\ \Omega_{\text{coll}} &= \boldsymbol{M}\boldsymbol{\Lambda}\boldsymbol{M}^{-1} \quad \text{(MRT)},\end{aligned}$$

τ represents the (single) relaxation time towards local equilibrium [19]; $\boldsymbol{M}$ and $\boldsymbol{\Lambda}$ are the transformation matrix and the (diagonal) matrix of the relaxation parameters, respectively: For the details on their formulation, the reader is addressed to Ref. [43]. More specifically, the $\boldsymbol{\Lambda}$ vector has $s_2 = s_{10} = s_{12} = s_{14} = s_{15} = s_{16} = \omega = \frac{2c_s^2}{c_s^2+\nu}$, and all the other free parameters equal to 1, where ν is the kinematic viscosity and c_s^2 is the squared lattice speed of sound. No special adjustments have been considered here because modifications on the $\boldsymbol{\Lambda}$ vector should not affect hydrodynamic behavior of the employed method. For both the SRT and the MRT formulations, the term $f_\alpha^{\text{eq}}(\mathbf{x},t)$ in Eq. (1) represents the distribution of (local) Maxwellian equilibrium, which is given by

$$\begin{aligned}f_\alpha^{\text{eq}}(\mathbf{x},t) = w_\alpha\rho(\mathbf{x},t)\Bigg[&\frac{\mathbf{c}_\alpha\cdot\mathbf{u}(\mathbf{x},t)}{c_s^2} + \frac{[\mathbf{c}_\alpha\cdot\mathbf{u}(\mathbf{x},t)]^2}{2c_s^4}\\ &- \frac{[\mathbf{u}(\mathbf{x},t)\cdot\mathbf{u}(\mathbf{x},t)]}{2c_s^2}\Bigg],\end{aligned} \tag{2}$$

in which $\rho(\mathbf{x},t)$ and $\mathbf{u}(\mathbf{x},t)$ are the hydrodynamic macroscopic density and velocity, respectively, and w_α represents the set of weights for the D3Q19 lattice [15,33]. From Eq. (1), macroscopic fluid density and velocity may be derived through the zeroth and the first population momenta, respectively, as follows:

$$\rho(\mathbf{x},t) = \sum_{\alpha=0}^{N_{\text{pop}}-1} f_\alpha(\mathbf{x},t), \quad \rho\mathbf{u}(\mathbf{x},t) = \sum_{\alpha=0}^{N_{\text{pop}}-1} \mathbf{c}_\alpha f_\alpha(\mathbf{x},t). \tag{3}$$

One among the main interesting *atouts* of the LBM lies in its effectiveness in dealing with nonideal multiphase flows [20]: The forcing term can be conveniently implemented in Eq. (1) to account for the phase interactions that trigger the macroscopic phase segregation. Among the various approaches proposed in the literature, we focus on the single-belt formulation of the pseudopotential Shan-Chen forcing [34,57], whose force reads

$$\mathbf{F}(\mathbf{x},t) = -G_0\psi(\mathbf{x},t)\sum_{\alpha=0}^{N_{\text{pop}}-1}\psi(\mathbf{x}+\mathbf{c}_\alpha\Delta t,t)\mathbf{c}_\alpha w_\alpha. \tag{4}$$

In Eq. (4), G_0 is the basic parameter which rules the interparticle interaction and $\psi(\mathbf{x},t)$ is the *pseudopotential*, a local functional of the fluid density [58],

$$\psi(\mathbf{x},t) = \rho_0\left[1-\exp\left(-\frac{\rho(\mathbf{x},t)}{\rho_0}\right)\right].$$

In this paper, we have fixed the reference density $\rho_0 = 1.0$: With this assumption, the interparticle strength G_0 is the only free parameter which fixes both the density ratio and the surface tension. Forcing schemes are different for the two collision operators; more in detail, for the SRT, starting from Eq. (4), the component of the interaction force along each direction can be evaluated and then used to shift the macroscopic velocities before evaluating the equilibrium distribution functions,

$$\mathbf{u}'(\mathbf{x},t) = \mathbf{u}(\mathbf{x},t) + \frac{\mathbf{F}(\mathbf{x},t)\tau}{\rho(\mathbf{x},t)}. \tag{5}$$

TABLE I. Main simulation parameters at $G_0 = -5.3$ and Oh $= 0.1$ as a function of ligament radius for the SRT.

R_0 (LU)	14	28	42	56	70	84	98
L_x	256	512	768	1024	1280	1536	1792
$L_y = L_z$	96	192	288	384	480	576	672
τ	0.67926	0.76297	0.83053	0.90311	0.97021	1.03776	1.10647
t_{cap}	335	912	1611	2380	3189	4015	4846
ρ_l	2.1167	2.1254	2.1348	2.1450	2.1557	2.1666	2.1775
ρ_v	0.0836	0.0900	0.0974	0.1059	0.1156	0.1264	0.1383
σ	0.05345	0.05775	0.06277	0.06848	0.07491	0.08206	0.08991

On the other hand, for the MRT scheme, we adopted the forcing scheme proposed in Refs. [38,42] where we compute the equilibrium momentum by means of the velocity evaluated as follows:

$$\mathbf{u}^b(\mathbf{x}, t) = \mathbf{u}(\mathbf{x}, t) + \frac{\mathbf{F}(\mathbf{x}, t)}{2\rho(\mathbf{x}, t)}. \tag{6}$$

For both considered collision operators, the EoS of the system may be written as follows:

$$P(\rho) = \rho c_s^2 + \frac{c_s^2 G_0}{2}\psi^2. \tag{7}$$

Before ending this methodological section, some remarks on the models used are in order. The main difference in between the two collision operators is that the SRT is solved into space, whereas the MRT projects the distribution functions into momentum space by means of the matrix **M** product. This technical passage allows for increasing the stability and robustness of the method itself. Regarding the equilibrium properties (i.e., density ratio, surface tension, etc.), it is well known that the basic Shan-Chen formulation is affected by some pathologies. Indeed, in the SRT formulation, both the surface tension and the density ratio depend on the relaxation parameter τ [57], whereas in the MRT formulation, they are decoupled from it. This is confirmed by Tables I and II. Furthermore, due to the forcing formulation, the surface tension is a function of the parameter G_0 itself, which causes a coupling between the EoS and the interface properties and results in the impossibility to tune surface tension independently of the EoS. Some extensions of the basic Shan-Chen force were designed to cure such pathology. Sbragaglia *et al.* [27] and Falcucci *et al.* [37] proposed to extend the range of interactions (i.e., multirange approach) of the Shan-Chen forces, allowing an independent tuning of the surface tension with respect to the EoS. Other studies followed, aimed at systematic characterizations and further improvements. For example, Yu and Fan [59] used a multirange approach to allow for nonuniform meshes and grid refinement close to nonideal interfaces; Huang *et al.* [60] systematically analyzed the impact of the multirange formulation on the equilibrium properties of nonideal interfaces; Li and Luo [61] proposed a modified approach by adding a source term to the LBM allowing the independent tuning of surface tension with respect to the EoS. The multirange extensions are here not explored; rather, we focus on the basic formulation of the pseudopotential approach to delve into some general considerations about "dynamical" spurious currents effects on macroscopic hydrodynamic phenomena. Indeed, the two LBM environments are here chosen as "representative" of two scenarios where spurious hydrodynamical effects exhibit a different modulation in space, in one case more localized in the pinching region and in another case localized away from the pinching region. In other words, the two LBM environments are not chosen to promote one with respect to the other but rather to raise a more general question on the dynamical distribution of nonhydrodynamical effects.

III. SIMULATIONS SETUP

We have performed the LBM simulations in a three-dimensional (3D) box of $L_xL_yL_z$ lattice sites. The Plateau-Rayleigh instability is triggered through a sinusoidal perturbation with a fixed amplitude and a constant wavelength (see Fig. 1). More specifically, the initial condition for the ligament radius is $r(x) = R_0 + \delta \sin(\frac{4\pi x}{L_x})$, where R_0 is the unperturbed ligament radius. The domain size and the ligament radius are chosen to accommodate roughly two wavelengths of the most unstable mode of the instability [6]. The perturbation δ is assigned the three different values of $R_0/30$, $R_0/20$, and $R_0/10$. The breakup phenomenon is driven by some characteristic parameters, and between them, the Ohnesorge number (Oh)

TABLE II. Main simulation parameters at $G_0 = -5.3$ and Oh $= 0.1$ as a function of ligament radius for the MRT.

R_0 (LU)	14	28	42	56	70	84	98
L_x	256	512	768	1024	1280	1536	1792
$L_y = L_z$	96	192	288	384	480	576	672
τ	0.67293	0.74445	0.79942	0.84575	0.88667	0.92350	0.95745
t_{cap}	347	981	1803	2775	3878	5098	6424
ρ_l	2.1086	2.1086	2.1086	2.1086	2.1086	2.1085	2.1085
ρ_v	0.0778	0.0779	0.0779	0.0779	0.0778	0.0778	0.0778
σ	0.04951	0.04952	0.04952	0.04955	0.04953	0.04953	0.04954

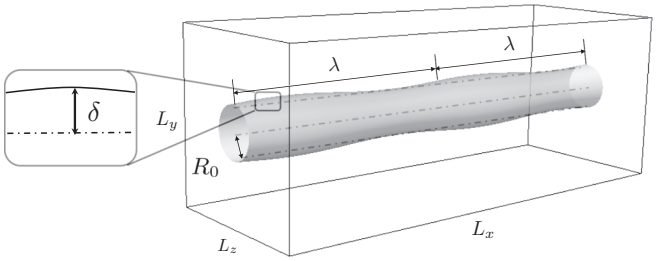

FIG. 1. Initial configuration for the numerical simulations. A cylindrical ligament of radius R_0 is perturbed with a sinusoidal wave along the axial (x) coordinate. The perturbation wavelength corresponds to the fastest growing mode of the Plateau-Rayleigh instability [6].

and the capillary time $t_{\rm cap}$ are defined as follows:

$$\mathrm{Oh} = \frac{\mu}{\sqrt{\rho_l \sigma R_0}}, \quad t_{\rm cap} = \sqrt{\frac{\rho_l R_0^3}{\sigma}}, \tag{8}$$

where ρ_l is the liquid density, μ is the dynamic viscosity, and σ is the surface tension. For our numerical simulations, the interparticle strength G_0 [27,37] has been fixed to -5.3 LU (lattice units hereafter), which allows a fair grid convergence study at changing the ligament radius R_0 from values comparable to the interface thickness to values much larger. Regarding the choice of the Ohnesorge number, a few remarks are in order. According to the literature on the breakup of liquid ligaments [62–64], it is known that, for $\mathrm{Oh} < 1$, instability phenomena of the liquid jet start to take place, causing the formation of pinched regions, which, eventually, lead to the breakup of the liquid column. To accomplish our analysis in the LBM framework, we have fixed $\mathrm{Oh} = 0.1$, which is a well-established value on the pinching breakup regime [65]. Moreover, through such a value, it is possible to have a set of corresponding numerical viscosities that grant the numerical stability of the LBM algorithm [15,33] as explained in the following. The ligament radius R_0 has been varied in the range of 14–98 LU. Table I reports the corresponding values of density ratio and surface tension retrieved with the SRT approach for the different values of R_0. To accurately evaluate the surface tension σ as a function of the ligament radius, we first carried out a set of steady-state simulations to perform the well known Laplace test [66]. With the SRT collision operator, the Laplace test requires accounting for the natural adaptation of σ to the kinematic viscosity value [57], whereas in the MRT framework, such an effect is absent. To retrieve a reliable value for the surface tension for all ligament radii reported in Table I, we have implemented an iterative procedure aimed at providing stable values for σ. More specifically, we chose a first attempt estimation for the viscosity, aimed at ensuring numerical stability; with the corresponding τ, we have performed the Laplace test according to three values of the static droplet radius, obtaining a first estimate of σ. By using the obtained value of surface tension in Eq. (8), we find the new viscosity value that meets the $\mathrm{Oh} = 0.1$ target: Since the values of σ, ρ_l, and ρ_v (vapor density) are intimately connected to that of τ in the SRT approach, we have iterated the above-described procedure until the relative error on two consecutive values of surface tension was less than 5%. For the MRT, no such procedure was needed as viscosity variations have a negligible impact on the algorithm. Once we acquired the asymptotic surface tension value for both collision operators, we performed simulations with flat interfaces to find the correct liquid and vapor densities corresponding to the simulation parameters. Finally, after this last set of simulations, we obtained all the input data needed to perform the ligament simulations. Table II displays the values of density ratio and surface tension obtained with the MRT collision operator: As is apparent from the comparison between Tables I and II, the values provided by the MRT display a negligible dependence of the physical properties on the employed computational grid.

Before closing this section, we notice that the breakup of a thin ligament has already been studied by means of an axisymmetric LBM formulation in Refs. [67–71]; in this paper, we extend the results already available in the literature by performing a 3D grid convergence analysis by analyzing the effect of different collision operators on the predictions of hydrodynamics and by performing a more detailed analysis on the properties of the breakup process.

IV. RESULTS

According to the parameters reported in Tables I and II, we have performed the numerical simulations for the breakup of the liquid ligament for $\delta = R_0/10$. In Fig. 2, we report results on the time evolution (up to the breakup point) and the breakup times $T_{\rm break}$ at changing the grid resolution. Note that the breakup time has been made dimensionless with respect to the capillary time $t_{\rm cap}$. For both collision operators, we observe a very neat trend of the breakup time increasing with the simulation resolution and, thus, with the initial radius R_0, in line with the numerical results in Ref. [72]. In our working conditions, sharp interface hydrodynamics predicts a dimensionless breakup time that is a function only of the Oh and δ (see Ref. [73] and references therein). Since the Oh and δ are fixed, the observed grid dependency cannot be explained in terms of sharp interface hydrodynamics, and it is an effect induced by the finite width of the interface. It naturally becomes the question of how much these finite width effects are hydrodynamical. To cope with this issue, one would need to use a diffuse interface hydrodynamic solver for the corresponding hydrodynamic equations predicted by the LBM [15,33]. Finite width effects are expected to be negligible for large resolutions, and one can use the results of sharp interface hydrodynamics (see Ref. [73] and references therein) for comparison. For the Ohnnesorge number used $\mathrm{Oh} = 0.1$, the breakup process is known to produce two mother droplets and two satellite droplets. In Fig. 2(b), the cases in which *stable* secondary droplets are found are reported with filled symbols. We would like to stress that only *stable* droplets have been considered, that is, secondary droplets that live for a period of time, at least, comparable to the capillary time $t_{\rm cap}$. It is known, in fact, that, in the pseudopotential framework of LBM multiphase flows, *small* droplets tend to be reabsorbed in the vapor phase as discussed in Refs. [40,74]. In our simulations, the SRT provides stable secondary droplets for $R_0 \geqslant 70$ LU, whereas the MRT collision operator provides

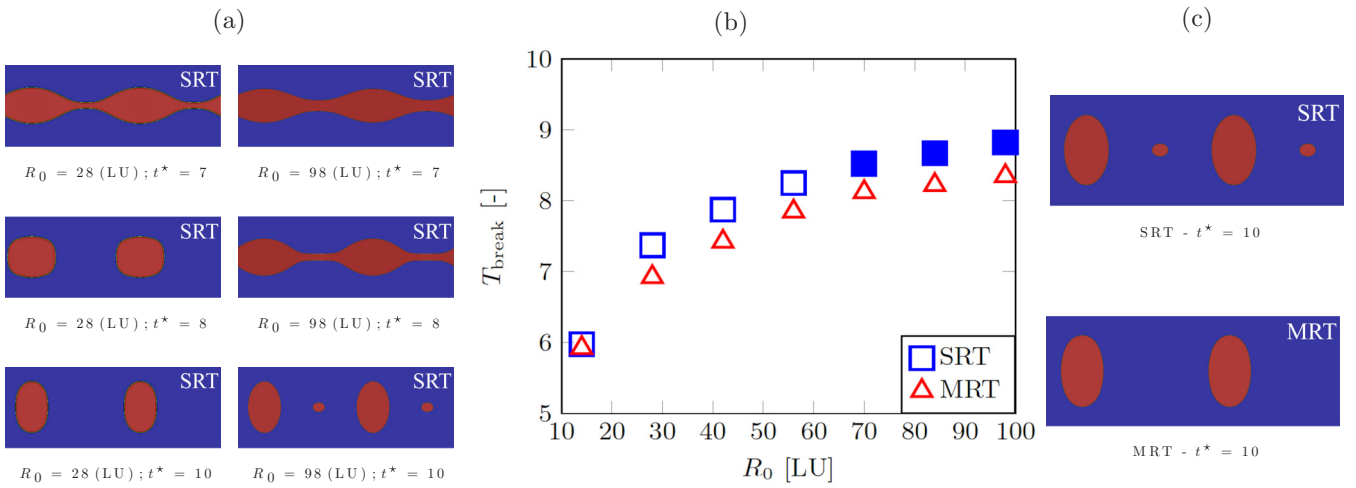

FIG. 2. Panel (a): We report the LBM density evolution as a function of the nondimensional time ($t^\star$) for the SRT collision operator and for different resolutions. Panel (b): We report the dimensionless breakup times as a function of the ligament radius for both the SRT and the MRT. The filled symbols refer to the presence of satellite droplets in postbreakup conditions. Panel (c): postbreakup conditions for both the SRT and the MRT.

secondary droplets that live considerably less than a single capillary time. Such a short-living feature is due to their initial diameters, which tend to be smaller with the MRT than with the SRT. By comparing the diameters obtained with the two collision operators to the analytic, numerical, and experimental results in the literature [50,75,76], we find that the SRT approach provides more accurate predictions. This surely calls for a careful comparison with the existing LBM data in the literature. Earlier investigation by Premnath and Abraham [67] used an axisymmetric LBM formulation with source terms embedded in the LBM dynamics in the Bhatnagar-Gross-Krook (BGK) approximation. The Carnahan-Starling EoS was used with a dynamic viscosity ratio of 4 between the liquid and the vapor phase. The authors report the formation of satellite droplets with an initial cylinder radius of 50 grid points (their Fig. 7), hence well below our largest resolutions used. Srivastava *et al.* [68] proposed an axisymmetric LBM formulation with the Shan-Chen force and the forcing scheme provided by the equilibrium shift, essentially the same as our forcing scheme for the SRT simulations. For $\mathrm{Oh} = 0.09$, they reported the formation of satellite droplets with a dynamic viscosity ratio of about 30, which is consistent with our results. Another axisymmetric LBM formulation proposed by Liang *et al.* [70] makes use of a phase field van der Waals model and adds the forcing term as a source to the BGK evolution. They use an initial cylinder radius with 60 grid points and report the presence of satellite droplets with a dynamic viscosity ratio of about 16.6. In the recent investigation by Liu *et al.* [71], the authors report numerical simulations with an axisymmetric LBM with a color-gradient model and a MRT collision operator, reporting the formation of satellite droplets. Finally, in the recent simulations by some of the authors with the Shan-Chen force for a multicomponent fluid and a MRT forcing scheme, the emergence of the satellite droplets was found [77]. These facts said, it is likely that the missed formation of satellite droplets in our MRT simulations originates from the chosen EoS and the choice of a viscosity ratio that sensibly differs from one.

Although at a very qualitative level, results in Fig. 2 provide a clue to a physically different behavior of the two collision operators with the SRT looking "more physical" than the MRT. This result is strange and counterintuitive since the Chapman-Enskog analysis predicts that SRT is affected by extra forcing-dependent stress contributions, which are large at large forces (i.e., close to interfaces). These observations stimulated further analysis on the quantitative comparisons between the numerical simulations and the theoretical predictions. To this aim, we kept the resolution fixed to the largest used in Fig. 2 and investigated the breakup time at changing δ. In Fig. 3, results of the numerical simulations are compared with the predictions of sharp interface hydrodynamics from Ref. [52] and linear stability analysis. Regarding the latter, the growth rate ω is considered as a function of both the wave number and the Ohnesorge number (see Eq. (28) in Ref. [6]). Knowing the growth rate, the breakup time in the linear approximation can be calculated from $T_{\mathrm{break}} = \ln(R_0/\delta)/\omega$

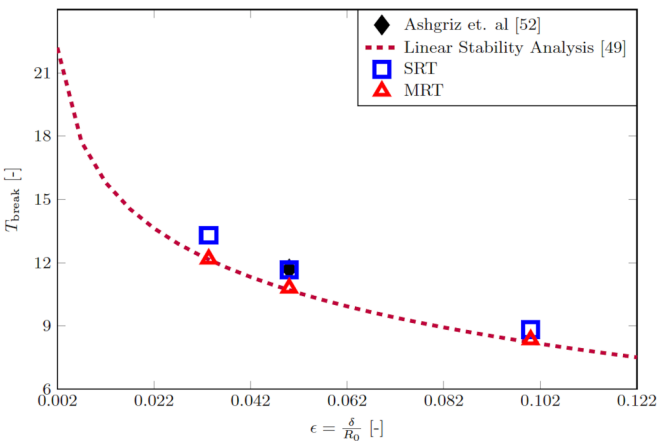

FIG. 3. Influence of the initial perturbation $\epsilon = \frac{\delta}{R_0}$ for the two collision operators on the nondimensional breakup time and comparison with literature data [52] and linear stability analysis prediction [49].

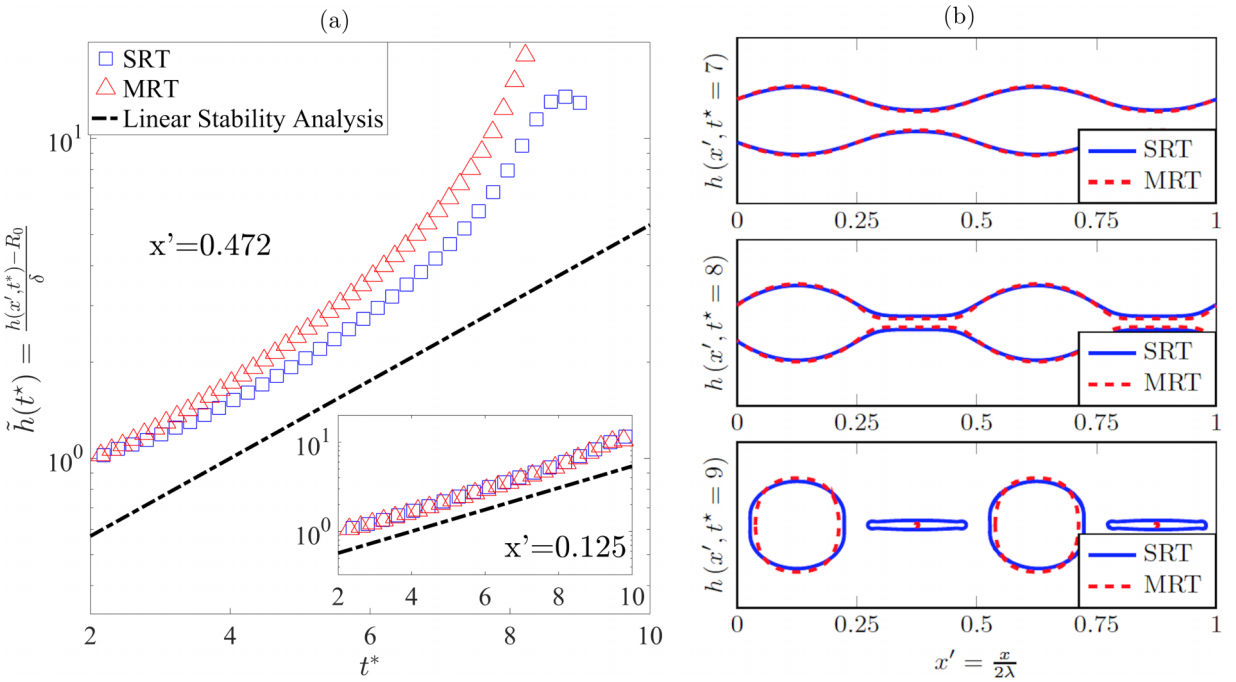

FIG. 4. Panel (a): Normalized perturbation with respect to the initial perturbation value at $x \approx L_x/2$ (and $x = L_x/8$ in the inset) as a function of nondimensional time. Panel (b): Three snapshots of interface evolution at $t^\star = 7$–9 both for the SRT and for the MRT.

[49,52]. We note that the MRT collision operator is well aligned with linear stability analysis reported in Ref. [49], whereas the SRT is practically overlapped with result presented in Ref. [52] where computation fluid dynamics Navier-Stokes (NS) simulations have been used for the same test case. In view of the results displayed in Figs. 2 and 3, one then asks where the mismatch between the two collision operators emerges, i.e., whether it is in the initial stage (where we are linearly unstable) or later at the pinch-off stage. To answer this question, we inspected the perturbation growth rate in the initial stage of the ligament destabilization and considered the ligament *silhouettes* for the whole dynamics up to breakup. The results are reported in Fig. 4. We observe that the initial destabilization process is the same and well in line with the prediction of sharp interface hydrodynamics. The difference between the two dynamics rather lies in the pinching regime. To have a deeper understanding of the ligament deformation near the breakup, we also look at the nondimensional "minimum" ligament radius as a function of the nondimensional time. Results are reported in Fig. 5. The minimum ligament radius is defined as the smallest radial coordinate in a configuration at a given time. We further make this quantity dimensionless by normalizing with the initial ligament radius. Note that sharp interface hydrodynamics predicts a linear trend of the minimum ligament radius [5,78] and the linear trend is more in line with the SRT dynamics than the MRT. It is worth nothing that the above presented method is characterized by a diffuse interface which tends to occupy few lattice points. Even though with increasing resolution the interface thickness tends not to influence results reliability, it is also true that for the maximum radius here considered (namely, $R_0 = 98$ LU) the interface still occupies 4 LU. Here, we consider that the interface is physically located exactly in the middle of the interface thickness. Thus, the LBM solver may be compared with the sharp interface hydrodynamics, whereas the interface width $h(x, t^\star)$ is greater than the half of interface thickness (about 2 LU). Below that threshold, there is no possibility to compare these two methods, and comparison would be formally incorrect. It is important to point out that the presented solvers do not introduce any special treatment so to reduce the interface thickness. Usually, such models are characterized by interfaces which occupy few sites but some technicalities have been developed so to reduce the number of nodes occupied by the interface. Moreover, this thickness cannot be zero, such as a sharp interface solver, and, its tuning will represent an additional degree of freedom while approaching these simulations. In the present paper, we have decided to modify the ligament radius while keeping

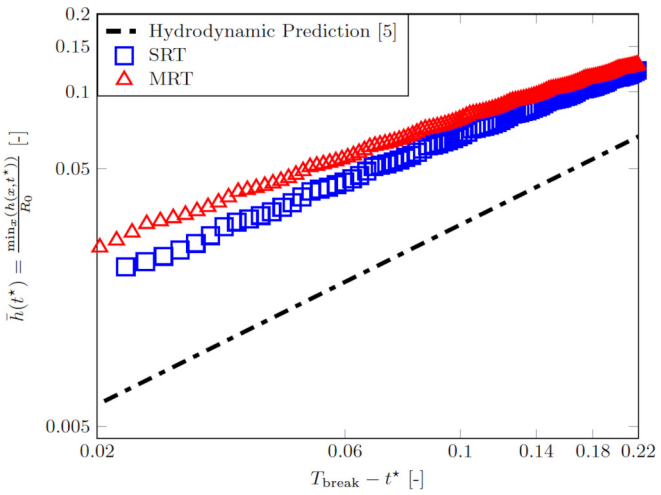

FIG. 5. Normalized minimum ligament height near the breakup time.

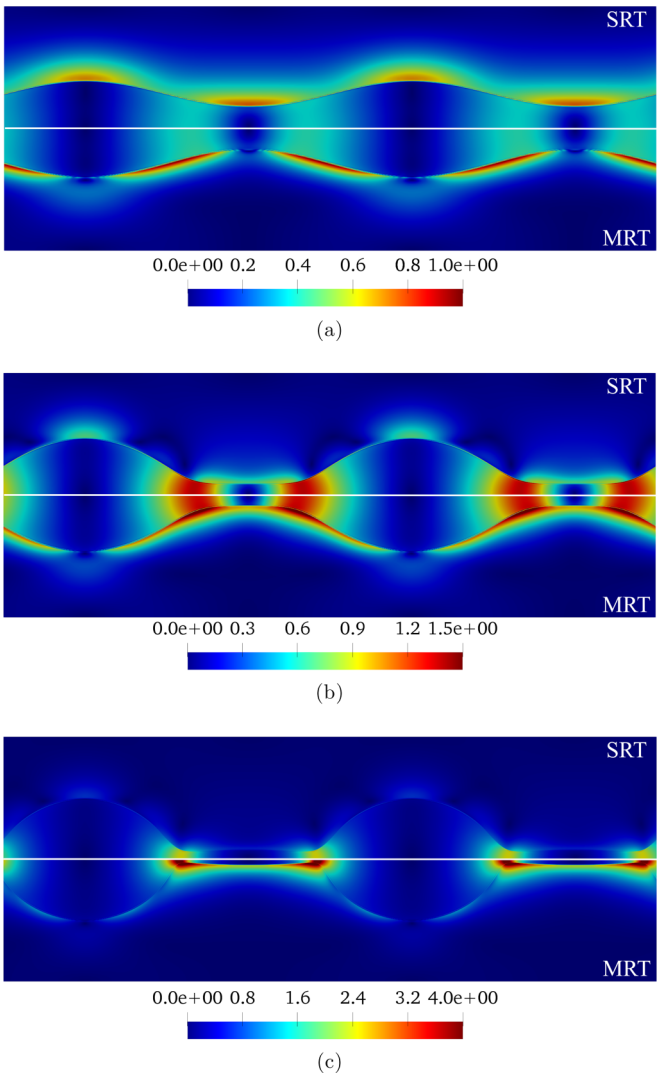

FIG. 6. Comparison of the time evolution of the normalized velocity magnitude according to the SRT and the MRT collision operators.

unchanged the interface thickness rather than modify the lattice sites occupied by the interface with the same ligament radius. To delve deeper into the problem, we compare the velocity profiles for the ligament during the time evolution of the surface instability leading to the liquid column breakup. Results are displayed in Fig. 6. The figure displays the dimensionless velocity magnitude $v* = \frac{|\mathbf{u}^b|}{R_0/t_{\text{cap}}}$ for both collision operators for selected times. To facilitate a comparison between the velocity distribution and the curvature profile, we compare the spatial distribution of the velocity field in both the MRT and the SRT at similar interface morphology. We observe that the dimensionless velocity profiles are different for the MRT and the SRT, both in spatial distribution and in magnitude. This difference in velocity greatly pertains to the vapor phase, and the velocity distributions are differently correlated to the curvature: whereas, for the SRT, the velocity localizes in the region of maximum curvature, for MRT, it localizes in the regions of maximum curvature changes. Moreover, when curvature increases, the velocity contributions increase. A quantitative assessment of how much the observed velocity distribution is spurious would require the solution of the full hydrodynamic equations in the presence of a vapor phase [6]. Nevertheless, the difference between the SRT and the MRT emerging from Fig. 6 suggests that both collision operators lead to spurious contributions that develop "dynamically" and whose spatial localization is different for the same curvature profiles. Specifically, if the spurious currents on the MRT are more localized at the pinch-off region, this can cause the breakup time to be different and the satellite droplets to be smaller after breakup. One could then reconsider the comments on the hydrodynamic recovery via the Chapman-Enskog theory: Although the SRT has extra terms with respect to the MRT in its Chapman-Enskog expansion, the mismatch may be originated by the fact that the impact of spurious currents is more *effective* in the present MRT implementation. In other words, the bulk equations are more correct in the MRT than in the SRT, but the interface boundary conditions are dynamically more spurious in the MRT than in the SRT. One could think of readsorbing this effect of spurious current in a modified stress tensor so that the dynamics of the MRT would be that of a system with a slightly different Ohnesorge number. At the largest resolution analyzed, however, this would not be possible: We do not observe any steady satellite droplets, whereas theory predicts them to exist [64]. Summarizing, for the specific test case analyzed, the pinching of the interface generates momentum, and it is significantly influenced by the distribution of spurious currents. As we may observe from Fig. 6, the MRT with this specific set of parameters shows a stronger concentration of velocities in the pinching region, whereas the SRT presents weaker interference. We think this is the reason why the breakup dynamics captured from the SRT better matches the expected results, despite presenting some possible lacks of consistency while reconstructing the NS equation.

V. CONCLUSIONS

We have investigated the dynamics of a liquid ligament perturbed via a Plateau-Rayleigh instability by means of the LBM. More specifically, we have considered two LBM collision operators, the SRT and the MRT, implemented in a multiphase numerical scheme based on the Shan-Chen EoS [34,36,57]. We have seen that numerical simulations display a neat asymptotic behavior in the limit where the interface thickness is sensibly smaller than the characteristic radius of the liquid ligament. Such behavior has been compared with the predictions of sharp-interface hydrodynamics [5,78] for both LBM environments. Adopting the same EoS, the two collision operators displayed a different behavior with the SRT granting results more adherent to the theoretical and experimental evidence from the literature, compared to the MRT. In particular, even if the breakup dynamics presents a very similar trend between the two collision operators in the early stages of the instability, the SRT provides a pinching evolution closer to the theoretical predictions with the eventual formation of a long-living secondary droplet after the ligament breakup, which we have not detected in the MRT environment. This difference is traced back to the dynamic distribution of spurious currents rising in the pinching region.

For the specific realizations of EoS adopted, the MRT—despite a higher numerical stability granted in the set of hydrodynamical parameters characterizing the simulation—displays a spurious currents pattern localized towards the flex of the ligament *silhouette* in the pinching region; the SRT, on the other hand, is characterized by a different distribution of the spurious velocities, which appear to be localized away from the pinching region, hence the dynamics of the ligament breakup is less affected by such a spurious pattern and provides results closer to the sharp-interface hydrodynamics.

On a more general perspective, some comments are in order. Our results show that, whenever spurious currents effects are weak in the pinching region, the LBM results can quantitatively match the ones obtained through the sharp-interface hydrodynamics from the initial perturbation destabilization up to the breakup point. The fact that our simulations with the SRT perform better than the MRT may well depend on the specificity of the parameters chosen here, causing dynamical spurious currents to distribute less in the pinching region. Although the issue of spurious currents has been pretty well detailed for "static" problems [27,32,60,79–81], very little is known about dynamical problems. Hence, we do not want to promote a collisional operator rather than the other; instead, we want to point out that different dynamical distributions of spurious currents may produce quantitatively different results. Of course, this is just a macroscopic property which obviously hides many nontrivial dependencies on the parameters and technical details of the models used. This also opens up future perspectives in determining the impact of the different parameters or choices at hand (e.g., EoS, thermodynamic consistency, surface tension coupling with EoS, collisional scheme, interface width, Knudsen effects, etc.) to obtain a "unifying view" on what are the causes behind the emergence of dynamical spurious currents.

ACKNOWLEDGMENTS

The numerical simulations were performed at the *Zeus* High Performance Computing (HPC) Facility at the University of Naples "Parthenope;" the *Zeus* HPC has been realized through the Italian Government Grant No. PAC01_00119 "MITO-Informazioni Multimediali per Oggetti Territoriali" with Professor E. Jannelli as the Scientist Responsible. This project has received funding from the Italian Government Program PRIN Grant No. 20154EHYW9. M.S. and X.X. thank the European Union's Horizon 2020 Research and Innovation Programme under the Marie Skłodowska Curie Grant Agreement No. 642069 for support.

[1] G. H. Yeoh, *Handbook of Multiphase Flow Science and Technology* (Springer, Berlin, 2015).
[2] A. Lefebvre and V. McDonell, *Atomization and Sprays,* 2nd ed. (CRC, Boca Raton, FL, 2017).
[3] K. K. Kuo, *Recent Advances in Spray Combustion: Spray Atomization and Drop Burning Phenomena* (American Institute of Aeronautics and Astronautics, Reston, VA, 1996).
[4] S.-P. Lin, *Breakup of Liquid Sheets and Jets* (Cambridge University Press, Cambridge, UK, 2003).
[5] J. Eggers, Phys. Rev. Lett. **71**, 3458 (1993).
[6] J. Eggers and T. F. Dupont, J. Fluid Mech. **262**, 205 (1994).
[7] F. Magaletti, F. Picano, M. Chinappi, L. Marino, and C. M. Casciola, J. Fluid Mech. **714**, 95 (2013).
[8] J. Eiken, B. Böttger, and I. Steinbach, Phys. Rev. E **73**, 066122 (2006).
[9] H. Ding, P. D. Spelt, and C. Shu, J. Comput. Phys. **226**, 2078 (2007).
[10] H. Ding and P. D. M. Spelt, Phys. Rev. E **75**, 046708 (2007).
[11] F. Gibou, L. Chen, D. Nguyen, and S. Banerjee, J. Comput. Phys. **222**, 536 (2007).
[12] P. Yue, C. Zhou, and J. J. Feng, J. Fluid Mech. **645**, 279 (2010).
[13] M. Wörner, Microfluid. Nanofluid. **12**, 841 (2012).
[14] J. Luo, X. Hu, and N. Adams, J. Comput. Phys. **284**, 547 (2015).
[15] S. Succi, *The Lattice Boltzmann Equation: For Complex States of Flowing Matter* (Oxford University Press, Oxford, 2018).
[16] Y. H. Qian and S. A. Orszag, Europhys. Lett. **21**, 255 (1993).
[17] F. J. Higuera, S. Succi, and R. Benzi, Europhys. Lett. **9**, 345 (1989).
[18] S. Ansumali, I. V. Karlin, and S. Succi, Physica A (Amsterdam) **338**, 379 (2004).
[19] R. Benzi, S. Succi, and M. Vergassola, Phys. Rep. **222**, 145 (1992).
[20] C. K. Aidun and J. R. Clausen, Annu. Rev. Fluid Mech. **42**, 439 (2010).
[21] G. Falcucci, S. Ubertini, D. Chiappini, and S. Succi, IMA J. Appl. Math. **76**, 712 (2011).
[22] G. Falcucci, G. Amati, V. K. Krastev, A. Montessori, G. S. Yablonsky, and S. Succi, Chem. Eng. Sci. **166**, 274 (2017).
[23] G. Falcucci, S. Succi, A. Montessori, S. Melchionna, P. Prestininzi, C. Barroo, D. C. Bell, M. M. Biener, J. Biener, B. Zugic *et al.*, Microfluid. Nanofluid. **20**, 105 (2016).
[24] G. Di Ilio, D. Chiappini, S. Ubertini, G. Bella, and S. Succi, Phys. Rev. E **95**, 013309 (2017).
[25] D. Chiappini, Int. J. Heat Mass Transf. **117**, 527 (2018).
[26] G. Bella, D. Chiappini, and S. Ubertini, SAE Int. J. Eng. **2**, 390 (2010).
[27] M. Sbragaglia, R. Benzi, L. Biferale, S. Succi, K. Sugiyama, and F. Toschi, Phys. Rev. E **75**, 026702 (2007).
[28] X. Shan and G. Doolen, J. Stat. Phys. **81**, 379 (1995).
[29] H. Zheng, C. Shu, and Y.-T. Chew, J. Comput. Phys. **218**, 353 (2006).
[30] M. Sbragaglia, R. Benzi, L. Biferale, H. Chen, X. Shan, and S. Succi, J. Fluid Mech. **628**, 299 (2009).
[31] C. E. Colosqui, G. Falcucci, S. Ubertini, and S. Succi, Soft Matter **8**, 3798 (2012).
[32] X. Shan, Phys. Rev. E **73**, 047701 (2006).
[33] T. Krüger, H. Kusumaatmaja, A. Kuzmin, O. Shardt, G. Silva, and E. M. Viggen, *The Lattice Boltzmann Method* (Springer, Berlin, 2017).
[34] X. Shan and H. Chen, Phys. Rev. E **47**, 1815 (1993).

[35] T. Lee and P. F. Fischer, Phys. Rev. E **74**, 046709 (2006).
[36] G. Falcucci, S. Chibbaro, S. Succi, X. Shan, and H. Chen, Europhys. Lett. **82**, 24005 (2008) .
[37] G. Falcucci, G. Bella, G. Chiatti, S. Chibbaro, M. Sbragaglia, and S. Succi, Commun. Comput. Phys. **2**, 1071 (2007).
[38] K. N. Premnath and J. Abraham, J. Comput. Phys. **224**, 539 (2007).
[39] A. L. Kupershtokh, D. A. Medvedev, and D. I. Karpov, Comput. Math. Appl. **58**, 965 (2009).
[40] G. Falcucci, S. Ubertini, and S. Succi, Soft Matter **6**, 4357 (2010).
[41] Q. Li, K. H. Luo, and X. J. Li, Phys. Rev. E **87**, 053301 (2013).
[42] D. Zhang, K. Papadikis, and S. Gu, Int. J. Multiphase Flow **64**, 11 (2014).
[43] S. Ammar, G. Pernaudat, and J.-Y. Trépanier, J. Comput. Phys. **343**, 73 (2017).
[44] M. Sbragaglia and D. Belardinelli, Phys. Rev. E **88**, 013306 (2013).
[45] M. Sbragaglia, R. Benzi, L. Biferale, S. Succi, and F. Toschi, Phys. Rev. Lett. **97**, 204503 (2006).
[46] J. W. S. Rayleigh, *Plateau (1873) Referenced in Theory of Sound* (Dover, NY, 1945), Vol. 11, p. 363.
[47] L. Rayleigh, Proc. London Math Soc. **1**, 4 (1878).
[48] L. Rayleigh, Proc. R. Soc. London **34**, 130 (1882).
[49] S. Chandrasekhar, *Hydrodynamic and Hydrodynamic Stability* (Oxford University Press, Oxford, 1961).
[50] D. Rutland and G. Jameson, Chem. Eng. Sci. **25**, 1689 (1970).
[51] M. Tjahjadi, H. A. Stone, and J. M. Ottino, J. Fluid Mech. **243**, 297 (1992).
[52] N. Ashgriz and F. Mashayek, J. Fluid Mech. **291**, 163 (1995).
[53] Z. Guo, C. Zheng, and B. Shi, Phys. Rev. E **65**, 046308 (2002).
[54] D. Chiappini, X. Xue, G. Falcucci, and M. Sbragaglia, *International Conference of Numerical Analysis and Applied Mathematics (ICNAAM 2017)*, AIP Conf. Proc. No. 1978 (AIP, New York, 2018), p. 420003.
[55] T. Krüger, F. Varnik, and D. Raabe, Comput. Math. Appl. **61**, 3485 (2011).
[56] G. Falcucci, E. Jannelli, S. Ubertini, and S. Succi, J. Fluid Mech. **728**, 362 (2013).
[57] X. Shan and H. Chen, Phys. Rev. E **49**, 2941 (1994).
[58] S. Chen and G. D. Doolen, Annu. Rev. Fluid Mech. **30**, 329 (1998).
[59] Z. Yu and L.-S. Fan, J. Comput. Phys. **228**, 6456 (2009).
[60] H. Huang, M. Krafczyk, and X. Lu, Phys. Rev. E **84**, 046710 (2011).
[61] Q. Li and K. H. Luo, Phys. Rev. E **88**, 053307 (2013).
[62] R. Schulkes, J. Fluid Mech. **309**, 277 (1996).
[63] J. Eggers and E. Villermaux, Rep. Prog. Phys. **71**, 036601 (2008).
[64] T. Driessen, R. Jeurissen, H. Wijshoff, F. Toschi, and D. Lohse, Phys. Fluids **25**, 062109 (2013).
[65] P. K. Notz and O. A. Basaran, J. Fluid Mech. **512**, 223 (2004).
[66] P.-G. De Gennes, F. Brochard-Wyart, and D. Quéré, *Capillarity and Wetting Phenomena: Drops, Bubbles, Pearls, Waves* (Springer Science+Business Media, New York, 2004).
[67] K. N. Premnath and J. Abraham, Phys. Rev. E **71**, 056706 (2005).
[68] S. Srivastava, P. Perlekar, J. H. M. ten Thije Boonkkamp, N. Verma, and F. Toschi, Phys. Rev. E **88**, 013309 (2013).
[69] S. Srivastava, T. Driessen, R. Jeurissen, H. Wijshoff, and F. Toschi, Int. J. Mod. Phys. C **24**, 1340010 (2013).
[70] H. Liang, Z. H. Chai, B. C. Shi, Z. L. Guo, and T. Zhang, Phys. Rev. E **90**, 063311 (2014).
[71] H. Liu, L. Wu, Y. Ba, G. Xi, and Y. Zhang, J. Comput. Phys. **327**, 873 (2016).
[72] A. Tiwari, H. Reddy, S. Mukhopadhyay, and J. Abraham, Phys. Rev. E **78**, 016305 (2008).
[73] T. Driessen and R. Jeurissen, Int. J. Comp. Fluid Dyn. **25**, 333 (2011).
[74] S. Chibbaro, G. Falcucci, G. Chiatti, H. Chen, X. Shan, and S. Succi, Phys. Rev. E **77**, 036705 (2008).
[75] P. Lafrance, Phys. Fluids **18**, 428 (1975).
[76] N. N. Mansour and T. S. Lundgren, Phys. Fluids A **2**, 1141 (1990).
[77] X. Xue, M. Sbragaglia, L. Biferale, and F. Toschi, Phys. Rev. E **98**, 012802 (2018).
[78] J. R. Lister and H. A. Stone, Phys. Fluids **10**, 2758 (1998).
[79] A. J. Wagner, Phys. Rev. E **74**, 056703 (2006).
[80] P. Yuan and L. Schaefer, Phys. Fluids **18**, 042101 (2006).
[81] D. N. Siebert, P. C. Philippi, and K. K. Mattila, Phys. Rev. E **90**, 053310 (2014).